Short-term variations of Mercury's Na exosphere observed with very high spectral resolution

François Leblanc, A. Doressoundiram, N. Schneider, S. Massetti, Mea Wedlund, A. López Ariste, C. Barbieri, V. Mangano, Gabriele Cremonese

▶ **To cite this version:**

François Leblanc, A. Doressoundiram, N. Schneider, S. Massetti, Mea Wedlund, et al.. Short-term variations of Mercury's Na exosphere observed with very high spectral resolution. Geophysical Research Letters, 2009, 36 (7), pp.L07201. 10.1029/2009GL038089 . hal-00375429

HAL Id: hal-00375429
https://hal.science/hal-00375429v1

Submitted on 11 Mar 2016

HAL is a multi-disciplinary open access archive for the deposit and dissemination of scientific research documents, whether they are published or not. The documents may come from teaching and research institutions in France or abroad, or from public or private research centers.

L'archive ouverte pluridisciplinaire **HAL**, est destinée au dépôt et à la diffusion de documents scientifiques de niveau recherche, publiés ou non, émanant des établissements d'enseignement et de recherche français ou étrangers, des laboratoires publics ou privés.

Short-term variations of Mercury's Na exosphere observed with very high spectral resolution

F. Leblanc,[1] A. Doressoundiram,[2] N. Schneider,[3] S. Massetti,[4] M. Wedlund,[1] A. López Ariste,[5] C. Barbieri,[6] V. Mangano,[4] and G. Cremonese[7]

Received 9 March 2009; revised 9 March 2009; accepted 20 March 2009; published 15 April 2009.

[1] Short time variations of Mercury's exosphere cannot be tracked easily from ground based observatories because of the difficulty of distinguishing them from Earth atmospheric effects. On July 13th 2008, using THEMIS solar telescope, we were able to simultaneously measure brightness, Doppler shift and width of the exospheric sodium D_2 emission line during half a day with a resolving power of ~370,000. Mercury's exosphere displayed an emission brightness peak in the Northern hemisphere which vanished in few hours and a more persistent Southern Hemispheric peak. The bulk Doppler shift of the exosphere suggests a period of strong escape from Mercury. The global changes of the Doppler shift and of the Doppler width suggest that a cloud of sodium atoms ejected before or at the beginning of our sequence of observations passed through THEMIS field of view moving anti-sunward. A preferentially southern ejection of sodium atoms leading to the observed persistent southern emission peak is consistent with the orientation of the Interplanetary Magnetic Field during that period. **Citation:** Leblanc, F., A. Doressoundiram, N. Schneider, S. Massetti, M. Wedlund, A. López Ariste, C. Barbieri, V. Mangano, and G. Cremonese (2009), Short-term variations of Mercury's Na exosphere observed with very high spectral resolution, *Geophys. Res. Lett.*, *36*, L07201, doi:10.1029/2009GL038089.

1. Introduction

[2] Mercury's sodium exosphere was observed by *Potter and Morgan* [1990] to be variable on timescales of an Earth day (that is ~10 minutes of Mercury solar time) with high latitude peaks in emission brightness appearing and disappearing in few Earth days. *Potter et al.* [2006] suggested that the solar wind might play a key role in producing such observed localized peaks and their short time variability. The reconnection between the interplanetary magnetic field (IMF) lines and Mercury's magnetic field lines would allow the solar wind to penetrate through Mercury's magnetospheric cusps [*Massetti et al.*, 2007]. The solar wind particles would then impact Mercury's surface inducing the sputtering of surface Na atoms leading to localized increases of the sodium exospheric density at high latitudes.

[3] Following *Massetti et al.* [2007], the solar wind density and velocity control the efficiency of the solar wind sputtering whereas the IMF orientation controls the size and position of the region where the solar wind particles impact Mercury's surface. When the radial component of the IMF is sunward and is the dominant component, the solar wind particles are predicted to preferentially impact the Southern hemisphere in a region whose size and position are driven by the two other components of the IMF. An opposite situation (anti-sunward IMF radial component) was encountered during MESSENGER first flyby with a more intense northern sodium emission than southern [*McClintock et al.*, 2008].

[4] The solar wind and IMF conditions changing on time scales much shorter than one Earth day, the exospheric signatures of the solar wind sputtering at Mercury should also change within few Earth hours. One of the problems with tracking short time variations from Earth is that, in few hours, Mercury is observed through various atmospheric conditions which are a significant potential source of misinterpretation.

[5] In this paper, we discuss the first simultaneous observations of Mercury's sodium brightness, Doppler shift and width during more than 10 continuous hours thanks to the very high resolution of THEMIS solar telescope and its capability to image Mercury's exosphere throughout daylight. Section 2 provides the information on these observations and the analysis performed, and sections 3 and 4 report discussion and conclusions, respectively.

2. Observations and Analysis

[6] THEMIS [*López Ariste et al.*, 2000] is a French-Italian solar telescope on the Canary Island of Tenerife with a 0.9 m primary mirror (with a central obscuration of 0.4 m) and a 15.04 m focal length. The slit size was 0.25" × 69.6" and the spectral resolution of 15.9 mÅ provided ~370,000 resolving power. One camera is used to measure the D_2 at 5890 Å Na emission line covering a spectral range of ~4 Å and is composed of 512 by 512 pixels at 7.8 mÅ/pixel spectral dispersion. The observation was obtained on the 13th July 2008 between 06:19 and 18:22 UT (08:19–20:22 local time). Mercury's true anomaly angle (TAA) was between 308.8 and 311.5°, the phase angle was between 67.3° and 65.4° and Mercury's radius (R_M) was 3.05". We were facing the dusk side of Mercury and were seeing 70% of Mercury's illuminated disk. Mercury's heliocentric distance was 0.33 AU and its heliocentric radial velocity was between −7.8 and −7.5 km/s (towards the Sun). The slit was oriented along

[1]LATMOS/IPSL, Université Versailles Saint Quentin, CNRS, Verrières-le-Buisson, France.
[2]LESIA, Observatoire de Paris, Meudon, France.
[3]LASP, University of Colorado, Boulder, Colorado, USA.
[4]IFSI, INAF, Rome, Italy.
[5]THEMIS, UPS853, CNRS, La Laguna, Spain.
[6]Department of Astronomy, University of Padova, Padova, Italy.
[7]Osservatorio Astronomico di Padova, INAF, Padova, Italy.

Copyright 2009 by the American Geophysical Union.
0094-8276/09/2009GL038089

Table 1. Subsequent Scans of July 13th 2008[a]

Scan n°	Time (UT, LT+2h)	Type of Scan	Seeing (″)	Average Emission (kR)	Average Doppler Shift (km/s)	Average Doppler Width (km/s)	North/South Hemispheric Emissions Ratio
3	06:19–06:50	HR, 9 positions separated by 0.5″	3.50 ± 0.28	N/A	−1.07 ± 0.02	2.90 ± 0.31	0.93
4	06:53–08:05	HR, 21 positions separated by 0.25″	1.50 ± 0.58	2.81 ± 0.28	−0.98 ± 0.02	2.79 ± 0.28	0.94
8	08:16–09:28	HR, 21 positions separated by 0.25″	1.33 ± 0.38	2.74 ± 0.15	−1.18 ± 0.01	2.84 ± 0.03	0.90
10	09:33–10:45	HR, 21 positions separated by 0.25″	1.50 ± 0.36	2.61 ± 0.15	−1.04 ± 0.01	2.87 ± 0.25	0.91
12	10:50–12:02	HR, 21 positions separated by 0.25″	1.67 ± 0.34	3.08 ± 0.13	−0.85 ± 0.01	2.78 ± 0.12	0.90
13	12:05–13:31	HR, 25 positions separated by 0.25″	1.83 ± 0.63	2.61 ± 0.32	−0.89 ± 0.01	2.74 ± 0.12	0.93
16	13:38–15:03	HR, 25 positions separated by 0.25″	1.67 ± 0.38	<2.60 ± 0.15	−0.89 ± 0.01	2.84 ± 0.27	0.78
17	15:05–16:31	HR, 25 positions separated by 0.25″	2.33 ± 0.47	2.73 ± 0.25	−0.97 ± 0.01	2.87 ± 0.27	0.81
21	16:55–17:38	LR, 12 positions separated by 0.5″	1.50 ± 0.42	3.28 ± 0.19	−0.98 ± 0.04	2.38 ± 0.45	0.82
22	17:39–18:22	LR, 12 positions separated by 0.5″	2.16 ± 0.53	3.11 ± 0.30	−1.05 ± 0.04	2.51 ± 0.45	0.75

[a]The average emission has been calculated by summing all the ADU measured within all the pixels of the scan, then by multiplying by the angular size of a pixel and then by dividing by the angular size of Mercury apparent disk. The average Doppler shift and width are calculated by fitting by a Gaussian distribution the sum of all spectra measured within all pixels with signal/noise ratio larger than 150 (Figure 3). Uncertainty on the Doppler shift and width (one standard deviation from Gaussian fit) should be considered as relative uncertainty. HR and LR are for high and low resolution respectively. Scan 16 did not cover the whole exosphere so that the average emission should be considered as a lower limit. For scan 3, coverage and seeing precluded a good estimate of the calibration. The method to calculate uncertainties on emission brightness and seeing is described by *Leblanc et al.* [2008].

Mercury's North/South axis and Mercury's exosphere was scanned with the slit automatically moved between each position in a direction perpendicular to the slit. Because the sky conditions were deteriorating, the two last scans were performed with lower resolution (220,000 and 27 mÅ spectral resolution) with a slit of 0.5" × 118" size. Details on each scan are provided in Table 1.

[7] The telescope provided tip-tilt corrections at ∼1 kiloHertz. At each slit position, ten individual exposures of twenty seconds were taken with negligible overhead for CCD readout and slit motions. The data were bias corrected and flat fielded. The flat field was obtained by observing the Sun using a special mode avoiding solar bright or dark spots. Spectral calibration was carefully performed, during the whole sequence of observation, using solar spectra obtained at four different times. The sky background was calculated from two segments at each end of the slit interpolated over the whole slit by fitting these two parts with a second degree polynomial. In order to subtract the reflected solar spectrum from Mercury's surface, we used the solar spectrum obtained for the closest atmospheric terrestrial conditions (similar air mass and zenith angle), shifted in wavelength, and scaled to the measurements. The exospheric emission line is then integrated subtracting an average background level calculated outside the emission line. We then fitted the emission line with a Gaussian function and derived the Doppler shift and the spectral full width at half maximum (FWHM) of the emission line after correction by the effect of the point spread function of the instrument. The Doppler shift of Mercury's exospheric line in Mercury's frame was determined using JPL/Horizon ephemerides. We estimated the uncertainty on the Doppler shift as ∼0.25 km/s. The brightness calibration is based on the Hapke theoretical model of the reflected solar light from Mercury's surface, which has the advantage of avoiding any uncertainty due to Earth's atmospheric absorption [*Sprague et al.*, 1997]. We have also developed a method to evaluate the uncertainty on the absolute calibration due to the uncertainty of position of the slit on Mercury's illuminated disk [*Leblanc et al.*, 2008].

3. Results

[8] Figure 1 shows the measured emission brightness during six of the best scans described in Table 1. The quality of the images is validated by our estimate of the seeing value and by the image of the continuum [*Leblanc et al.*, 2008]. As shown in Table 1, 4th column, these scans were obtained for comparable atmospheric conditions. As displayed in Figure 1, there are distinct Northern and Southern exospheric peaks structure during scans 4 and 8, followed by a progressive disappearance of the northern peak in less than five hours, whereas the southern peak is still evident up to scan 22 (more than 11 hours later, see also Table 1 last column). The average emission brightness intensity (Table 1: fifth column) displays minima during scans 10 and 13–16, a significant maximum during scan 12 and an increase from scan 17 up to the end of the observation.

[9] In Figure 2, the spatial distribution of the Doppler shift associated to each plot of Figure 1 is shown. In Table 1 (6th column) we also provide the Doppler shift of the sum

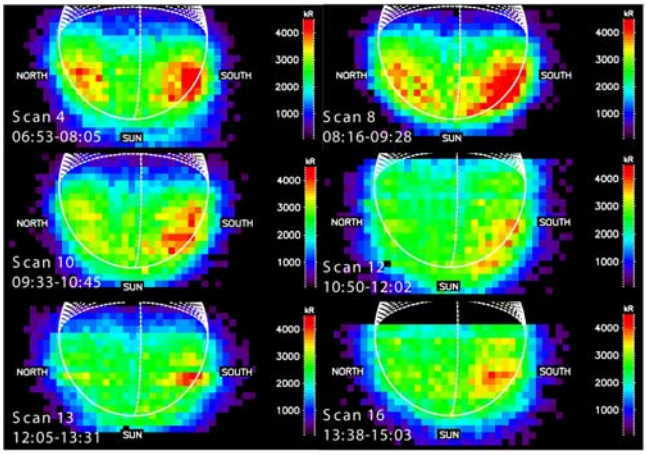

Figure 1. Emission brightness during the six consecutive scans on the 2008/07/13. Mercury's disk is plotted. The white dashed lines are longitudes on the nightside region. The scan of Mercury is done from bottom to top of each panel. Only pixels where the signal/noise ratio was greater than 150 are plotted.

of all pixels for each scan (Figure 3). This Doppler shift is always negative and displays minima at scan 8 and at the end of the observation and a maximum at scan 12. A positive Doppler shift corresponds to atoms moving away from the observer and mainly anti-sunward. The Doppler shift as seen from Earth depends on the angle between the line of sight and the vector normal to the surface, the sodium atoms being ejected preferentially perpendicularly to the surface. Since sodium atoms are also pushed anti-sunward by the solar radiation pressure, such a Doppler shift will also depend on the angle between the line of sight and the solar zenith angle. For quiet conditions, we should observe a globally negative Doppler shift of the atoms along the line of sight with maxima at the solar limb and in the anti-solar direction (bottom and top parts of each panel) and

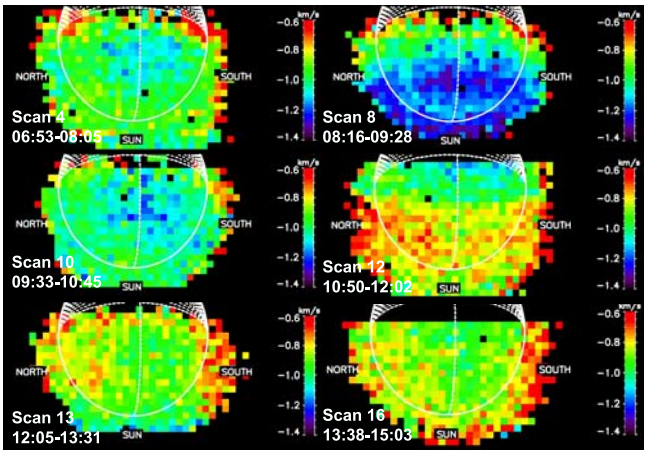

Figure 2. Doppler shift of the Na D_2 emission line in Mercury's frame. A positive Doppler shift means that the Na atoms move on average away from the observer whereas a negative Doppler corresponds to Na atoms moving towards the observer. Only pixels where the signal/noise ratio was greater than 150 are plotted.

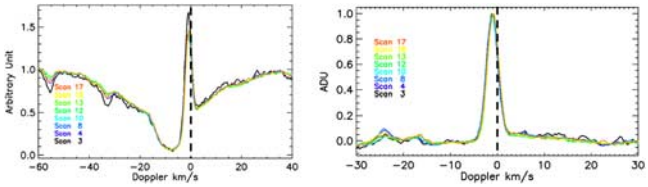

Figure 3. Spectra of the measured signal obtained by summing all pixels with signal/noise ratio larger than 150. (left) The sky contribution to the measured spectra was subtracted but not the solar reflected light on Mercury's surface. (right) Same as Figure 3 (left) but with the solar reflected light on Mercury's surface subtracted. Each spectrum is plotted in Mercury's exospheric frame (zero Doppler shift, vertical dashed line).

a minimum at the sub-Earth point. Such a minimum of the Doppler shift at the center of the apparent disk is observed in Figure 2, for scans 4, 8 and 10 as well as for scans 13 to 17. A globally negative Doppler shift (Figure 3) implies also that a significant part of the observed exosphere was not dominantly gravitationally bounded to Mercury. In the contrary, we should have observed a globally null Doppler shift in Mercury's frame.

[10] *Leblanc et al.* [2008] observed an enlargement of the Doppler spectral line in association with peak of emission brightness and interpreted this as the signature of an energetic process of ejection. The Doppler width distribution during the 6 scans displayed Figures 1 and 2 is shown in Figure 4. We observe a slightly hotter southern hemisphere than the northern during the whole sequence of observation. Two episodes of increase of the Doppler width appear also to occur during scans 8 and 10 and during scans 16 and 17 in Figure 4 (also evident in the average Doppler width displayed 7th column of Table 1). Therefore, during these two periods of maximum Doppler width, it is probable that solar wind sputtering increased leading to a local increase of the Doppler width and to the Doppler shift minima during scan 8 and less evidently during scans 16–17. The association between Doppler width and peak of emission is not as clear for these observations as for the one reported by *Leblanc et al.* [2008]. This can be explained by worse seeing conditions, Mercury being also closer to the Earth in 2007, but also as a signature of the weakness of the energetic processes during our observation. Moreover, most of the atoms producing the southern and northern brightness peaks were probably ejected before the start of our observation, so that they either already moved away from the region of ejection for the most energetic particles as suggested by Figure 4 or partially thermalized by reimpacting the surface.

[11] Scan 12 is the only scan which does not display a clear minimum of the Doppler shift at the center of the apparent disk. We interpret it as the path of another cloud of sodium moving anti-sunward, with positive Doppler shift as suggested by the peak of the average brightness, Figure 1, during scan 12 but without brighter high latitude peaks. Such atoms may have been ejected before scan 10, as suggested by the increase of the Doppler width. The rate of ejection towards the observer between scans 4 and 10, should have peaked during scan 8, as suggested by the contrast between the emission brightness of the high latitude

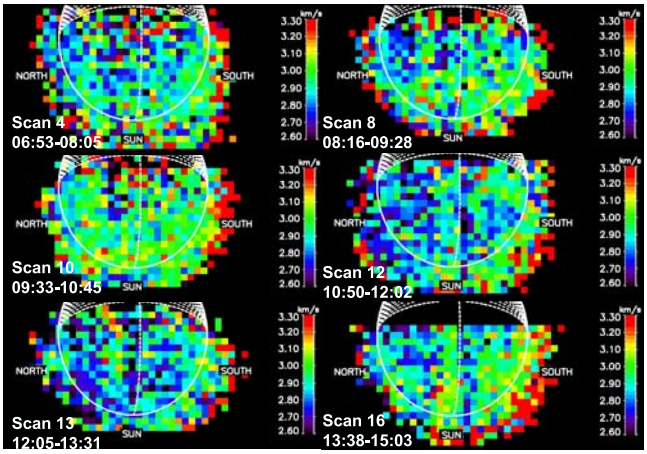

Figure 4. Doppler Width of the spectral Na D_2 emission line. Only pixels where the signal/noise ratio was greater than 150 are plotted.

peaks with the rest of the exosphere. An episode of strong ejection during scan 8 is also suggested by the minimum of the Doppler shift close to the subsolar region. The minimum of average emission brightness during scan 10 (Table 1, 5th column) could have been due to those atoms ejected before scan 10 being slowed down by solar radiation pressure (around -180 cm s^{-2} at TAA = 310° [*Smyth and Marconi*, 1995]) down to a null velocity with respect to the Sun (and therefore passing through a minimum of the number of solar photons a sodium atom could scatter) before moving anti-sunward. The minimum of the Doppler width during scan 13 would be then the signature of a quiet period during which energetic ejection decreased. If f_1 represents the total number of atoms of the bulk exosphere with a Doppler shift V_1 and f_2 the atoms in the cloud moving with a Doppler shift of V_2, then the average measured Doppler shift observed during scan 12 would be equal to $V = (V_1 \times f_1 + V_2 \times f_2)/(f_1 + f_2)$ if the exosphere is assumed to be optically thin. V_1 is the average Doppler shift measured when no second population is present, that is $V_1 \sim -0.9$ km/s (scan 13). The cloud population when ejected from the surface should have a velocity of the order of -1.2 km/s (scan 8) and should reimpact the surface with a similar velocity, that is, $V_2 \sim +1.2$ km/s, implying, $f_1 \sim 41 \times f_2$ ($V = -0.85$ km/s for scan 12). Therefore, apart from any consideration of scattering efficiency, the increase of exospheric atoms needed to produce the Doppler shift signature observed during scan 12 (f_2) should represent only few percent of the total exospheric sodium atomic population (f_1) in good agreement with the total emission brightness variation (Table 1, 5th column). A similar episode of ejection apparently occurred after scan 16 (from the Doppler width increase) but will be not discussed here because the conditions of observation worsened after scan 16.

[12] In summary, the presence of a persistent peak in emission brightness in the southern hemisphere during more than 11 hours seems to be due to at least two consecutive events of solar wind sputtering and preferentially in the Southern hemisphere. The Northern peak remained visible from Earth for a few hours which suggests that after being initiated by a dramatic increase of the ejection rate, probably before the start of our observation (if not we would have seen a signature in the Doppler width during scan 4), the peak in exospheric density progressively fades away during several hours being partially maintained by recycling and induced diffusion in the surface. In the contrary, the apparently more persistent southern peak might be explained by one or more subsequent episodes of preferentially southern ejection as indicated by the Doppler width signatures. These episodes of ejection were probably weak as suggested by the lack of significant variation of the total emission brightness.

[13] It is possible to infer the variation and orientation of the IMF during the period of our observations by using Advanced Composition Explorer measurements (ACE, which was 20 Earth radii above the equatorial plane) and the Wilcox Solar Observatory solar data (WSO). At that time, WSO indicates that both Earth and Mercury were above the equatorial plane by 4° and 2.5° respectively. The correction due to the Earth–Sun–Mercury angle as well as to the propagation time of the solar wind between the Earth and Mercury was evaluated using the interplanetary discontinuity linked to the equatorial coronal hole recorded by the SoHO EIT instrument as a marker. Mercury on the July 13th appears to have encountered a period of variable sign of the radial magnetic field component but with long period of sunward and strong values. As stated in the introduction, a strong sunward radial component should induce a preferentially bombardment of the Southern hemisphere as supported by our observation.

4. Conclusions

[14] Eight consecutive images of the brightness, Doppler shift and width of Mercury's exospheric D_2 emission line have been obtained during almost eleven hours by THEMIS solar telescope using very high resolving power (~370,000). Two high latitude peaks in emission brightness were visible at the beginning of our sequence of observation. The Northern hemispheric peak vanished during the first five hours of observation whereas the Southern peak lasted during the whole sequence. In the same time, the Doppler shift changed significantly as well as the Doppler width. These observations suggest that a strong ejection event occurred before or at the beginning of our sequence of observations producing in particular the Northern hemispheric peak. Such an event leads to the formation of a cloud of sodium atoms probably initially ejected towards the Sun, then slowed down and accelerated in the anti-sunward direction by the solar radiation pressure. This first event of ejection was then followed probably by a second episode of increased ejection rate preferentially from the Southern hemisphere.

[15] *Baumgardner et al.* [2008] and S. Okano et al. (personal communication, 2008) have recently observed Mercury's sodium tail and reported the presence of localized peak of density along the tail that they interpreted as potentially short time variation in Mercury's exosphere. We here show that indeed Mercury's exosphere significantly change in less than a few Earth hours.

References

Baumgardner, J., J. Wilson, and M. Mendillo (2008), Imaging the sources and full extent of the sodium tail of the planet Mercury, *Geophys. Res. Lett.*, *35*, L03201, doi:10.1029/2007GL032337.

Leblanc, F., A. Doressoundiram, N. Schneider, V. Mangano, A. López Ariste, C. Lemen, B. Gelly, C. Barbieri, and G. Cremonese (2008), High latitude peaks in Mercury's sodium exosphere: Spectral signature using THEMIS solar telescope, *Geophys. Res. Lett.*, *35*, L18204, doi:10.1029/2008GL035322.

López Ariste, A., J. Rayrole, and M. Semel (2000), First results from THEMIS spectropolarimetric mode, *Astron. Astrophys.*, *142*, 137–148.

Massetti, S., S. Orsini, A. Milillo, and A. Mura (2007), Modelling Mercury's magnetosphere and plasma entry through the dayside magnetopause, *Planet. Space Sci.*, *55*, 1557–1568.

McClintock, W. E., et al. (2008), Mercury's exosphere: Observations during MESSENGER's first Mercury flyby, *Science*, *321*, 92–94.

Potter, A. E., and T. H. Morgan (1990), Evidence for magnetospheric effects on the sodium atmosphere of Mercury, *Science*, *248*, 835–838.

Potter, A. E., R. M. Killen, and M. Sarantos (2006), Spatial distribution of sodium on Mercury, *Icarus*, *181*, 1–12.

Smyth, W. H., and M. L. Marconi (1995), Theoretical overview and modeling of the sodium and potassium atmospheres of Mercury, *Astrophys. J.*, *441*, 839–864.

Sprague, A. L., R. W. H. Kozlowski, D. M. Hunten, N. M. Schneider, D. L. Domingue, W. K. Wells, W. Schmitt, and U. Fink (1997), Distribution and abundance of sodium in Mercury's atmosphere, 1985–1988, *Icarus*, *129*, 506–527.

C. Barbieri, Department of Astronomy, University of Padova, Vicolo Osservatorio 2, I-35122 Padova, Italy.

G. Cremonese, Osservatorio Astronomico di Padova, INAF, Vicolo Dell'Osservatorio 5, I-35122 Padova, Italy.

A. Doressoundiram, LESIA, Observatoire de Paris, 5, place Jules Janssen, F-92195 Meudon CEDEX, France.

F. Leblanc and M. Wedlund, LATMOS/IPSL, Université Versailles Saint Quentin, CNRS, Réduit de Verrières BP 3, F-91371 Verrières-le-Buisson CEDEX, France. (francois.leblanc@latmos.ipsl.fr)

A. López Ariste, THEMIS, UPS853, CNRS, C/Via Lactea s/n, E-38200 La Laguna, Spain.

V. Mangano and S. Massetti, IFSI, INAF, Via del Fosso del Cavaliere, 100, I-00133 Roma, Italy.

N. Schneider, LASP, University of Colorado, Campus Box 392, Boulder, CO 80309-0392, USA.